

ornl

ORNL/TM-10669

**OAK RIDGE
NATIONAL
LABORATORY**

MARTIN MARIETTA

Theoretical Study of the Folded Waveguide

G. L. Chen
T. L. Owens
J. H. Whealton

OAK RIDGE NATIONAL LABORATORY

CENTRAL RESEARCH LIBRARY

CIRCULATION SECTION

ACORN ROOM 115

LIBRARY LOAN COPY

DO NOT TRANSFER TO ANOTHER PERSON

If you wish someone else to see this
report, send us some with report and
the library will arrange a loan.

OPERATED BY
MARTIN MARIETTA ENERGY SYSTEMS, INC.
FOR THE UNITED STATES
DEPARTMENT OF ENERGY

Printed in the United States of America. Available from
National Technical Information Service
U.S. Department of Commerce
5285 Port Royal Road, Springfield, Virginia 22161
NTIS price codes—Printed Copy: A03; Microfiche A01

This report was prepared as an account of work sponsored by an agency of the United States Government. Neither the United States Government nor any agency thereof, nor any of their employees, makes any warranty, express or implied, or assumes any legal liability or responsibility for the accuracy, completeness, or usefulness of any information, apparatus, product, or process disclosed, or represents that its use would not infringe privately owned rights. Reference herein to any specific commercial product, process, or service by trade name, trademark, manufacturer, or otherwise, does not necessarily constitute or imply its endorsement, recommendation, or favoring by the United States Government or any agency thereof. The views and opinions of authors expressed herein do not necessarily state or reflect those of the United States Government or any agency thereof.

ORNL/TM-10669
Dist. Category UC-426, UC-427

Fusion Energy Division

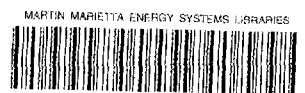
**THEORETICAL STUDY OF THE
FOLDED WAVEGUIDE**

**G. L. Chen
T. L. Owens*
J. H. Whealton**

*McDonnell Douglas Astronautics Company, St. Louis.

Date Published—January 1988

Prepared by the
OAK RIDGE NATIONAL LABORATORY
Oak Ridge, Tennessee 37831
operated by
MARTIN MARIETTA ENERGY SYSTEMS, INC.
for the
U.S. DEPARTMENT OF ENERGY
under contract DE-AC05-84OR21400



3 4456 0275138 7

CONTENTS

ABSTRACT	v
I. INTRODUCTION	1
II. COMPUTATIONAL METHOD AND CHARACTERIZATION OF FIELDS	2
III. COMPARISON WITH EXPERIMENTAL MEASUREMENTS	3
IV. CONCLUSIONS	4
REFERENCES	5

ABSTRACT

We have applied a three-dimensional (3-D) algorithm for solving Maxwell's equations to the analysis of folded waveguides used for fusion plasma heating at the ion cyclotron resonance frequency. A rigorous analysis of the magnetic field structure in the folded waveguide is presented. The results are compared to experimental measurements. Optimum conditions for the folded waveguide are discussed.

I. INTRODUCTION

A low-frequency, compact waveguide has been proposed by Owens¹ for use in ion cyclotron resonance heating (ICRH) of fusion plasmas. This new ion cyclotron resonant frequency (ICRF) antenna is known as a folded waveguide coupler.^{1,2} As shown in Fig. 1, the folded waveguide coupler is basically a rectangular waveguide that has been transversely folded to form a compact structure and to reduce the resonant frequency. At the Oak Ridge National Laboratory (ORNL), experiments on the folded waveguide are being carried out on the Radio Frequency Test Facility.

As stated in Ref. 1, the folded waveguide has three important merits as an ICRH antenna. First, it is a compact, all-metal, low-frequency antenna that can be used in larger fusion devices, such as Tore Supra, the Tokamak Fusion Test Reactor (TFTR), and the Compact Ignition Tokamak (CIT). Second, a polarizing plate at the mouth of the waveguide can eliminate the E_{\parallel} field and behave like the conventional Faraday shield used in loop antennas. Third, a shorting plate placed at the back of the antenna will ensure that the electric field of the wave in the

ORNL-DWG 85-3407A FED

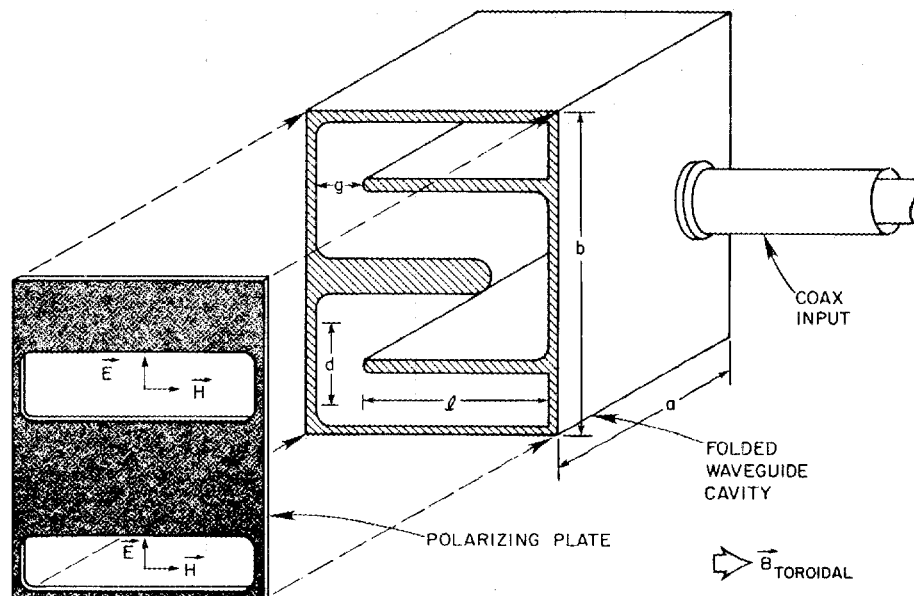


Fig. 1. Folded waveguide ICRF coupler concept.

coupling apertures is small while the H_{\parallel} field is near maximum, thereby improving the plasma-antenna match with a low plasma surface impedance (E_{\perp}/H_{\parallel}).

Owens calculated the field structures by unfolding the folded waveguide into a rectangular waveguide and imposing a periodic E_x field on the boundary.¹ These calculations qualitatively verify the folded waveguide concept. However, a more precise and rigorous calculation is needed to confirm the concept and support the high-power waveguide design.

For this purpose, we apply a 3-D Maxwell's equation solver³ to calculate the field structures and the resonant frequency in a realistic folded waveguide geometry. Our method has several basic merits. A finite difference method is used with a successive overrelaxation (SOR) convergence scheme and a method of treating boundaries that allows the cavity to have an arbitrary shape. Second, either Dirichlet or Neumann boundary conditions are easily considered. Third, it is much easier to treat 3-D problems with our method than with the transmission-line matrix (TLM) method,⁴ which leads to a rather complex network containing series as well as shunt nodes. The results are compared with experimental measurements in vacuum.⁵ To study breakdown problems, we adopt a much simpler two-dimensional (2-D) model. We find from the 2-D analysis that the geometry, shape, and thickness of the vanes play an important role in avoiding voltage breakdown problems.

In Sec. II, we describe the theory and the computational method. We present the results of the study and compare them with experimental measurements in Sec. III. Conclusions are given in Sec. IV.

II. COMPUTATIONAL METHOD AND CHARACTERIZATION OF FIELDS

Many methods are now available for solving problems concerning waveguides. These include the equivalent circuits method, the variational principle method, and the direct solution of Maxwell's equations, either analytically or numerically. The appropriate method depends on the complexity of the problem involved and the kinds of information needed. In this work, we are mainly interested in finding the full-wave fields and the resonant frequency in the waveguide with exact folded waveguide geometry. Hence, we adopt the method of a direct numerical solution of Maxwell's equations.

It is well known that the electromagnetic fields of a free-space cavity are governed by two equations:

$$\left(\nabla^2 + \mu_0 \epsilon_0 \frac{\omega^2}{c^2}\right) \vec{E} = 0 \quad (1)$$

and

$$\left(\nabla^2 + \mu_0 \epsilon_0 \frac{\omega^2}{c^2}\right) \vec{H} = 0 \quad , \quad (2)$$

where $\nabla^2 = (\partial^2/\partial x^2) + (\partial^2/\partial y^2) + (\partial^2/\partial z^2)$ is the Laplacian operator, ω is the frequency, c is the speed of light, $\mu_0 = 4\pi \times 10^{-7}$ H/m is the permeability of free space, and $\epsilon_0 = 8.8542 \times 10^{-12}$ F/m is the permittivity of free space. The fields \vec{E} and \vec{H} are related by two of Maxwell's equations,

$$\nabla \times \vec{E} = i \frac{\omega}{c} \vec{B} \quad (3)$$

and

$$\nabla \times \vec{B} = -i \mu \epsilon \frac{\omega}{c} \vec{E} \quad . \quad (4)$$

They are also constrained by the other two Maxwell's equations,

$$\nabla \cdot \vec{E} = 0 \quad (5)$$

and

$$\nabla \cdot \vec{B} = 0 \quad . \quad (6)$$

With proper boundary conditions for a cavity, we can solve Eq. (1) or Eq. (2) analytically or numerically. Then we find the other set of solutions by using Eq. (3) or Eq. (4).

In this paper, we use the finite difference method with a successive overrelaxation (SOR) convergence scheme³ to solve Eq. (1) or Eq. (2) numerically. The system is first solved for the longitudinal component (H_z) of Eq. (2), with the following boundary conditions. On the surface where \hat{n} is perpendicular to \hat{z} ,

$$\frac{\partial H_z}{\partial n} = 0, \quad (7a)$$

and on the surface where \hat{n} is parallel to \hat{z} ,

$$H_z = 0, \quad (7b)$$

where \hat{n} is the unit vector outward normal to the surface of the boundary S . These conditions are shown schematically for a rectangular waveguide cavity in Fig. 2. The resonant frequency of either the folded or the rectangular cavity can be determined from the longitudinal wave equation without solving the transverse wave equation. In practice, some excitation of the TM mode within the cavity is possible

ORNL-DWG 85-3476R FED

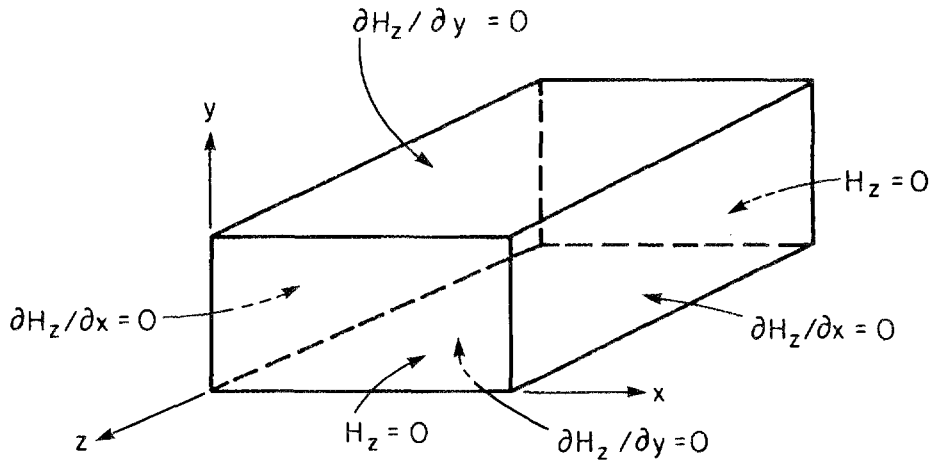


Fig. 2. Schematic representation of the boundary conditions of H_z .

because of imperfect shielding by the polarizing plate of the folded waveguide coupler. This effect is assumed to be small and is neglected in the present analysis.¹ Since Maxwell's equations [Eqs. (3) and (4)] in vacuum are linear in \vec{E} and \vec{B} , the principle of superposition of the mode is valid. When we know H_z , we can find the transverse fields H_x and H_y for the TE mode from⁶

$$H_x = \frac{\partial/\partial x(\partial H_z/\partial z)}{k^2 - k_z^2} \quad (8)$$

and

$$H_y = \frac{\partial/\partial y(\partial H_z/\partial z)}{k^2 - k_z^2} \quad (9)$$

A folded waveguide with parameters $a = 21.75$ cm, $b = 14.5$ cm, $g = 3.05$ cm, and $\ell = 9.15$ cm is used as an example here. The numerical mesh size is $24 \times 57 \times 10$. It takes about 60 min of Cray cpu time to achieve the convergent solution. The three components of \vec{H} for the lowest frequency mode throughout the entire folded waveguide with both ends closed are shown in the 3-D plots of Fig. 3. The boundary layer of the waveguide has been removed from all our 3-D plots to reveal the

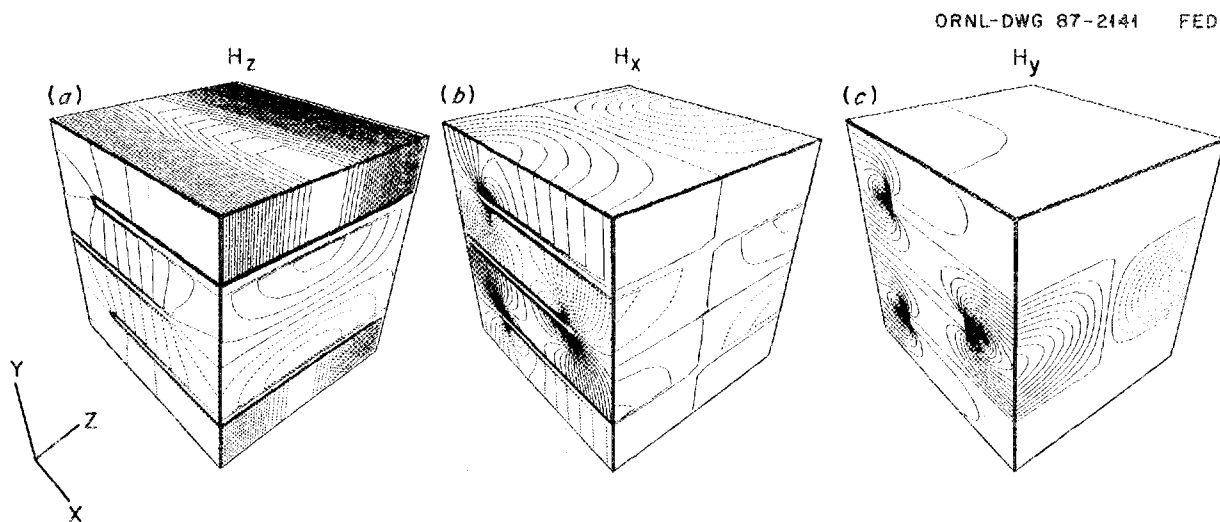


Fig. 3. Three-dimensional contour plots of constant field magnitude for (a) H_z , (b) H_x , and (c) H_y components of the lowest frequency mode in a folded waveguide with both ends closed. The solid lines indicate the positive field; the dashed lines, the negative field. The amplitude is normalized to the maximum value. The parameters are $a = 21.75$ cm, $b = 14.5$ cm, $g = 3.05$ cm, and $\ell = 9.15$ cm.

inside field structure. The resonance frequency is 762 MHz, which is below the resonance frequency of a rectangular waveguide with the same dimensions for reasons explained below. Experiments with a waveguide on this scale have been made.⁵ The results show very close agreement with the calculated resonance frequency and \vec{H} field, as discussed in Sec. III.

Figure 4 is a schematic representation of the \vec{H} field structure of the fundamental TE mode in a folded waveguide and in its equivalent unfolded rectangular waveguide. By comparing the H_z field of the folded waveguide with the H_z field of the corresponding unfolded waveguide, which is four times larger in the x -direction and one-fourth as large in the y -direction, we can easily see that the field structure for the lowest order mode within the unfolded waveguide is folded inside the coupler.

ORNL-DWG 87-2437 FED

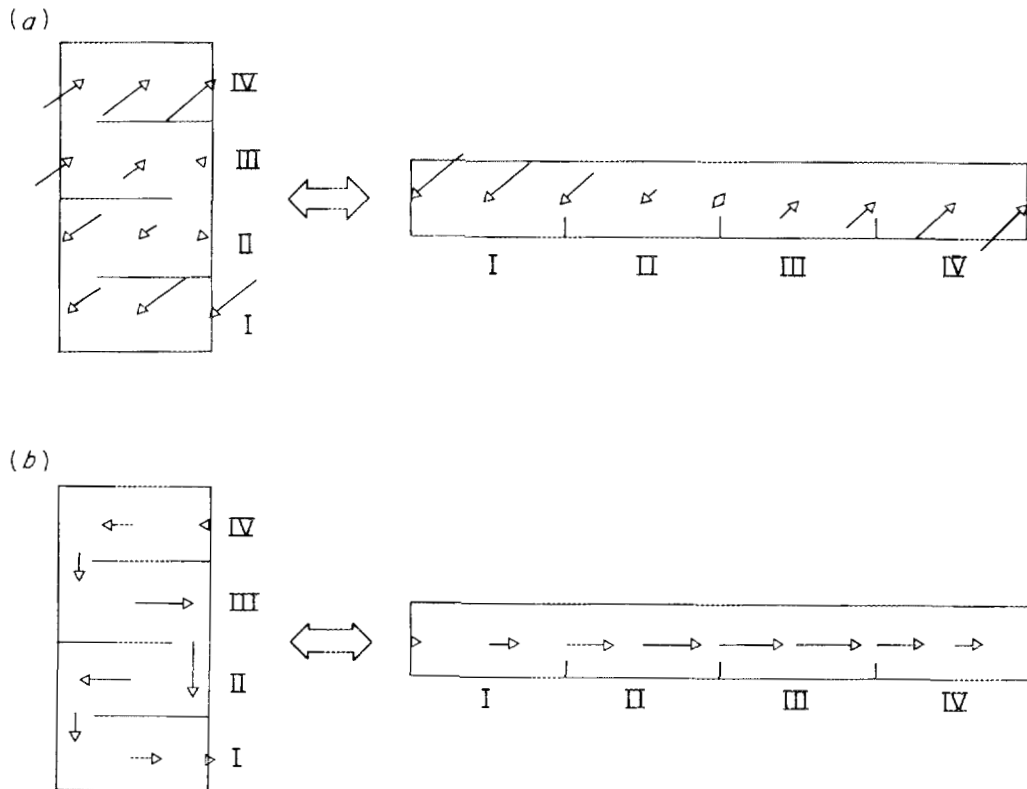


Fig. 4. Schematic comparison of the folded waveguide field and the equivalent rectangular waveguide. (a) The longitudinal fields H_z . (b) The transverse field $\vec{H}_\perp = \vec{H}_x + \vec{H}_y$.

This is the main advantage of the folded waveguide coupler—it produces resonance modes similar to those of rectangular waveguides in a device that is much smaller physically. This is very important for fusion experimental devices that do not have large access ports. In a rectangular waveguide, the longer the x -dimension, the lower the resonant frequency when the other two dimensions are fixed. Hence, we expect that in the folded waveguide, the more vanes inserted, the lower the frequency. The vanes appear to play the role of extending the wave path inside the waveguide. Our study shows that the resonant frequency of a folded waveguide is even lower than that of the equivalent unfolded waveguide. The resonant frequency is a function of the number of vanes and their length and thickness; increasing the length and the thickness of vanes can reduce the resonant frequency. A useful empirical formula for approximation of the resonant frequency is

$$f = \frac{c}{2} \left\{ \frac{n_x^2}{[(m+1)\ell + md]^2} + \frac{n_y^2}{b^2} + \frac{n_z^2}{a^2} \right\}^{1/2}, \quad (10)$$

where n_x , n_y , and n_z are the eigennumbers of the equivalent unfolded rectangular cavity, b and c are the y and z dimensions of the cavity, m is the number of vanes, ℓ is the length of the vane, and d is the distance between the adjacent sections measured from the center (see Fig. 1).

Figure 5 is a plot of the lowest resonant frequency versus the gap between the tip of the vane and the wall for a $30.0 \times 48.7 \times 97.5$ -cm folded waveguide with six vanes, each 2.29 cm thick. The minimum frequency occurs for a gap of 5 cm. All of the resonant frequencies are below those for the two extreme cases: (a) a folded waveguide with no gap (gap = 0 cm), which corresponds to six independent rectangular waveguides ($30.0 \times 6.95 \times 97.5$ cm), and (b) a folded waveguide with no vanes (gap = 30 cm), which corresponds to a large rectangular waveguide ($30.0 \times 48.7 \times 97.5$ cm). For case (a) the mode is TE_{101} with a resonance frequency of 523 MHz, and for case (b) the mode is TE_{011} with a resonance frequency of 344 MHz.

A nearly direct correspondence can be drawn between the longitudinal fields of a folded waveguide and of the equivalent unfolded waveguide. A similar correspondence can be drawn between their transverse fields. In the fundamental TE mode, the transverse field of an equivalent unfolded waveguide is simply $\vec{H}_\perp = \vec{H}_x$, because

ORNL-DWG 86C-2231AR FED

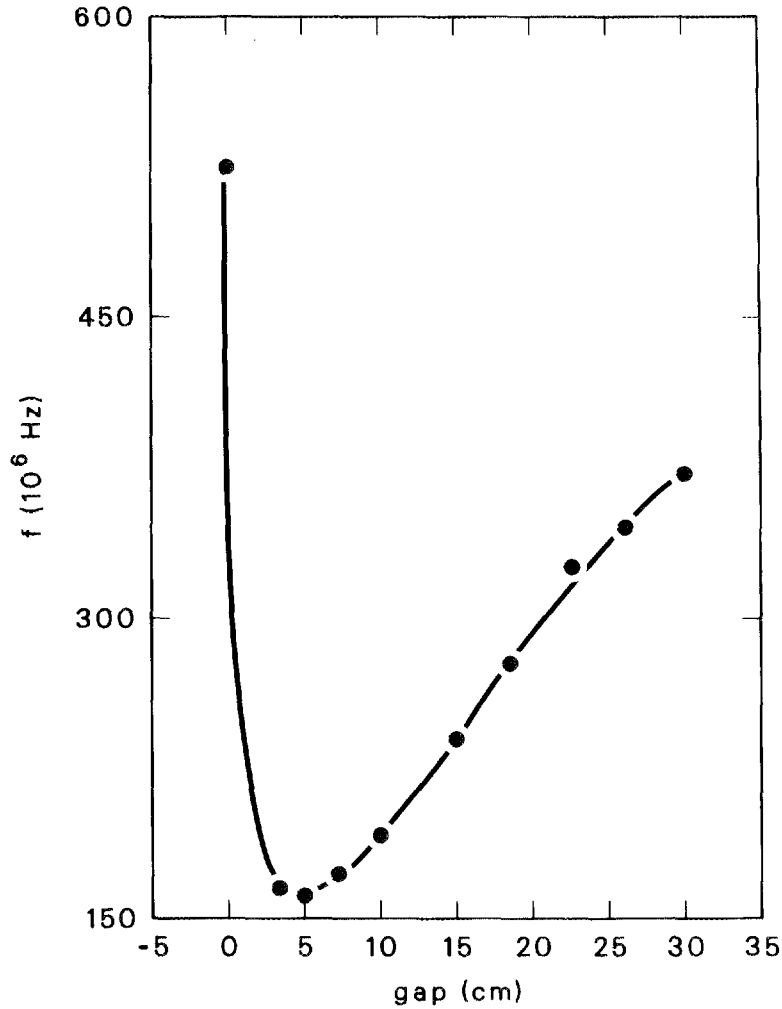


Fig. 5. Lowest resonant frequency as a function of gap size for a $30 \times 48.75 \times 97.5$ cm folded waveguide with six vanes, each 2.29 cm thick.

the H_y component vanishes everywhere, as shown in Fig. 4. However, in the folded waveguide the transverse field is the sum of \vec{H}_x and \vec{H}_y ; that is, $\vec{H}_\perp = \vec{H}_x + \vec{H}_y$. While H_x almost vanishes between the vanes and the wall, H_y reaches its maximum value there. Our results show that the amplitudes of H_x and H_y are comparable. The H_y field connects the H_x fields between adjacent sections. Otherwise, the H_x field would be squeezed out by the vanes, and each section would behave like an independent cavity. The total transverse field is thus folded in the waveguide, as is the longitudinal field.

Because H_x is the toroidal magnetic field in the plasma, the plasma heating efficiency is largely determined by the character of this field. An important feature of H_x is the reversal of its direction in adjacent sections of the waveguide; this does not occur for H_y or H_z . Basically, the alternation of field direction would produce field destructive interference in front of the coupler when the distance between adjacent sections d is shorter than the distance to the plasma surface. This field cancellation would significantly reduce the heating efficiency. A polarizing plate is needed to cover every other section to ensure a nearly unidirectional field at the plasma surface.

Another interesting feature of the transverse field structure is that there are strong fields near the vane tips because of the sharp edges of the vanes. In Sec. III, we discuss elimination of these fields by smoothing the vane edges to avoid voltage breakdown.

A folded waveguide with one open end has been studied because this type of waveguide can serve as a low-frequency, compact reentrant waveguide. This structure could also be used to launch fast waves by rotating it 90 deg from its fast-wave orientation. In this case, however, a Faraday shield might have to be added to the front of the coupler to shield the E_{\parallel} fields produced between coupler vanes. The shield would have to be placed some distance in front of the vanes in order to avoid contact with the vanes. The three components of the lowest frequency mode H field are plotted in Fig. 6. In this case, the H_z field has maximum values on the open end and vanishes at the closed end to produce a quarter-wavelength structure in the z -direction. The H_y and H_x fields have minimum values at the open end and maximum values at the closed end.

The situation with a polarization plate or a Faraday shield at the plasma/coupler interface creates a very complicated boundary condition, which is difficult to solve and is properly the subject of future work. In this paper we focus on the simpler solution displayed in Figs. 3 and 6, which can be readily compared with experiment.⁵ It should be noted that even these relatively simple solutions are likely to be too complex to solve by analytic means.

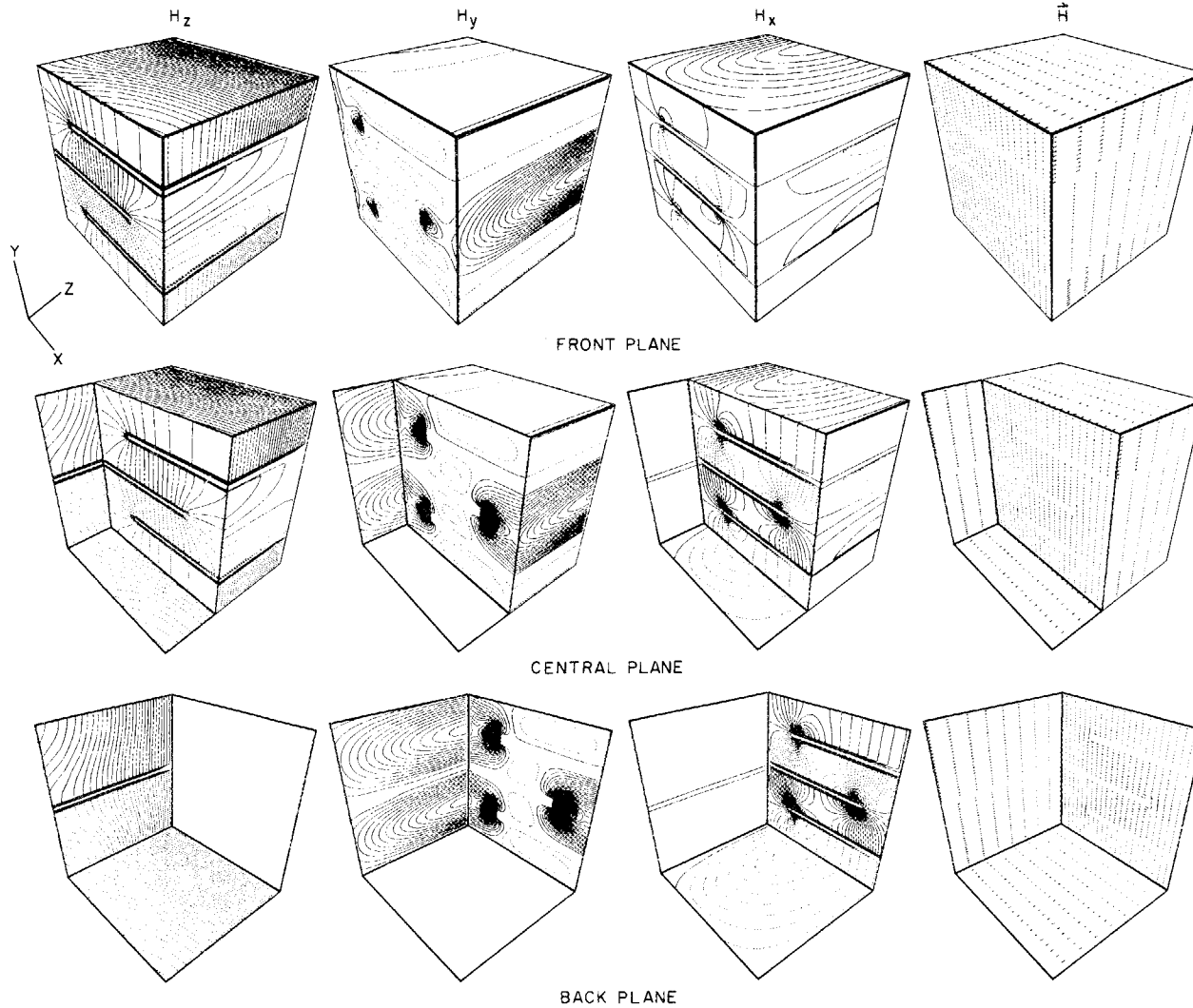


Fig. 6. The contour plots of constant field magnitude for H_z , H_y , and H_x components of the lowest frequency mode in a folded waveguide with one end open. The solid lines indicate the positive field; the dashed lines, the negative field. The amplitude is normalized to the maximum value. The parameters are $a = 21.75$ cm, $b = 14.5$ cm, $g = 3.05$ cm, and $\ell = 9.15$ cm.

III. COMPARISON WITH EXPERIMENTAL MEASUREMENTS

The folded waveguide coupler has been tested at low power⁵ to verify the predicted free-space field pattern within the structure. A four-section coupler, similar to that shown in Fig. 1, was studied. Holes were drilled in the front plate, through which a small loop probe was inserted for measuring the direction and relative magnitude of the fields. The lowest measured resonant frequency was 768 MHz, in good agreement with the resonance frequency of 762 MHz obtained from our 3-D calculation. The result from Eq. (10) is 750 MHz.

Figure 7 shows that the calculated and measured relative magnitudes of the \vec{H} field near the front plate are also in good agreement. The magnitude is symmetric about the central vane. The field within the two central sections is roughly double that of the two outside sections. The analogous features of the calculated and measured field directions are displayed in Fig. 8. They show that the field reverses

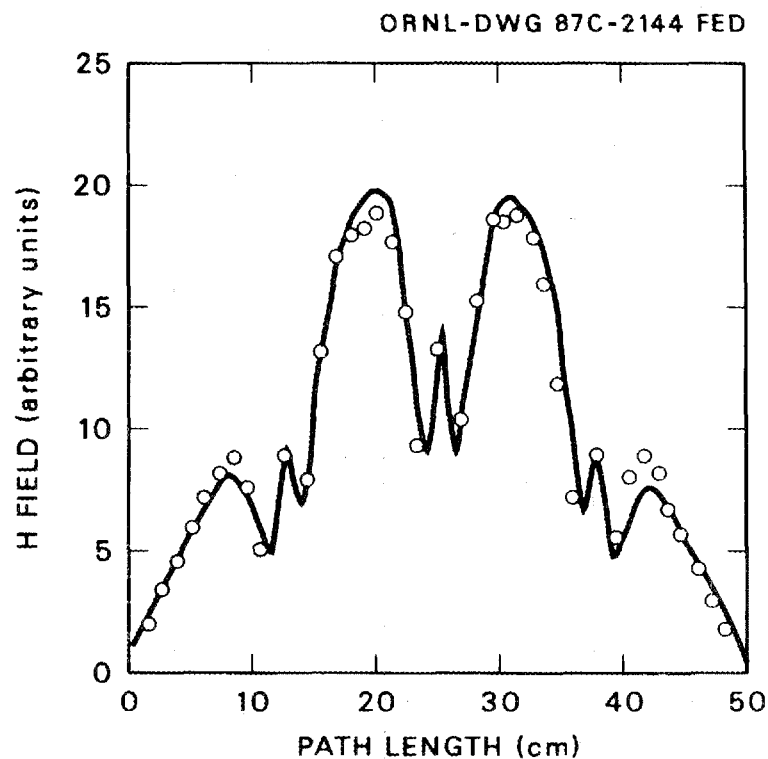


Fig. 7. Calculated and measured relative magnitudes of the H field near the front plate.

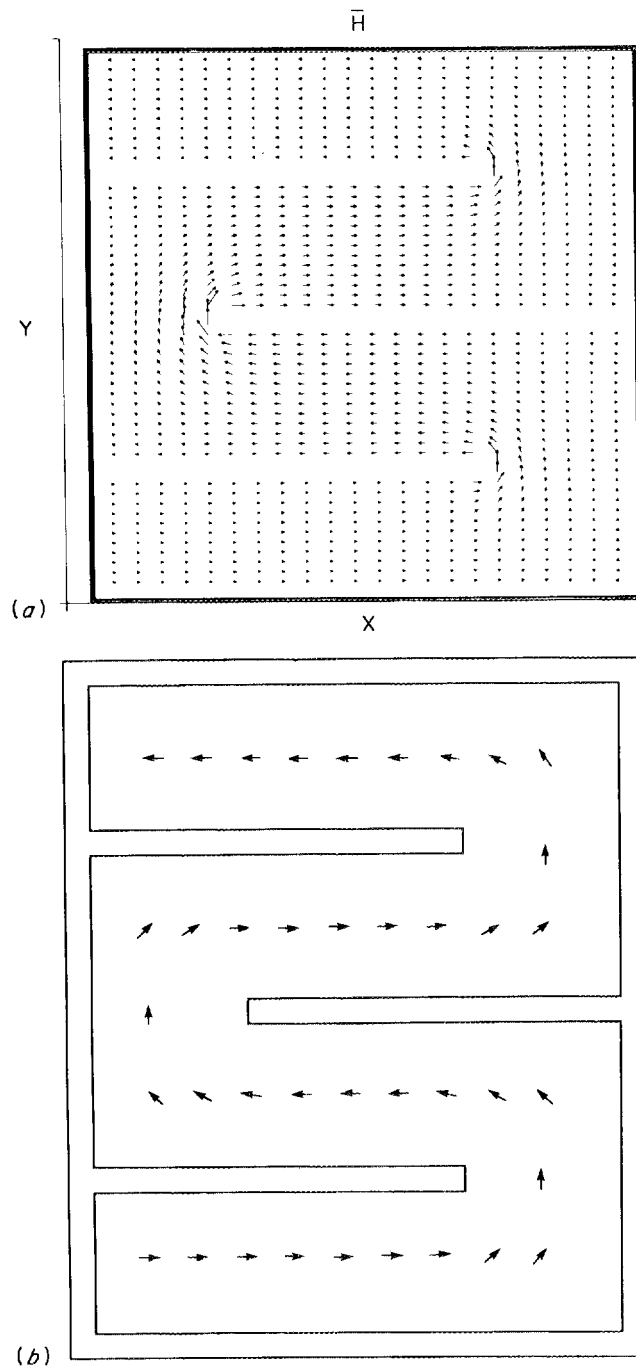


Fig. 8. Calculated and measured transverse magnetic field (\vec{H}_{\perp}) directions, showing field reversal in adjacent sections. Field strength is indicated by length of tails on arrows.

in adjacent sections. Overall, the calculated features of the field are nearly identical to the measured features.

In Fig. 8(a), we find that the field near the tips of the vanes is much higher than elsewhere. This strong field could cause a voltage breakdown problem at high power. For simplicity, and with no degradation of the physics, we use a 2-D approximation (Fig. 9) of a single-vane folded waveguide with two different vane tip shapes to study the maximum transverse electric field E_{\perp} . Figure 9(a) shows the vector plot of E_{\perp} for a rectangular tip, and Fig. 9(b) shows the vector plot of E_{\perp} for a semispherical tip. The vane thickness (t) was one-third of the height (b). The semispherical tip has much smoother E_{\perp} fields around the vane surface, but the rectangular tip has very high E_{\perp} fields near its corners. (Near the rectangular corners, E_{\perp} has been smoothed out as a result of the finite mesh size; the actual field is much higher than that shown.) The maximum $|E_{\perp}|$ for the semispherical tip vs the ratio of thickness to height is shown in Fig. 10. The results indicate optimum conditions when $t/b \approx 0.25$. In this calculation, we have assumed that the energy flow $\int \vec{E} \times \vec{H}^* dA$ and the distance between the vane's tip and the cavity wall (g) remain constant when t/b is varied in order to maintain an approximately constant resonant frequency. The curve in Fig. 10 approaches a constant value when $t/b \rightarrow 1$, because the cavity cross section approaches a finite limiting area, approximately equal to $b \times g$ (refer to Fig. 1 for dimensions). However, if we increase the length ℓ as well as the vane thickness t to keep the gap between the vane and the cavity wall uniform everywhere, then the curve in Fig. 10 should rise rapidly when $t/b \rightarrow 1$ because the cross section goes to a small value and the maximum $|E_{\perp}|$ becomes very large.

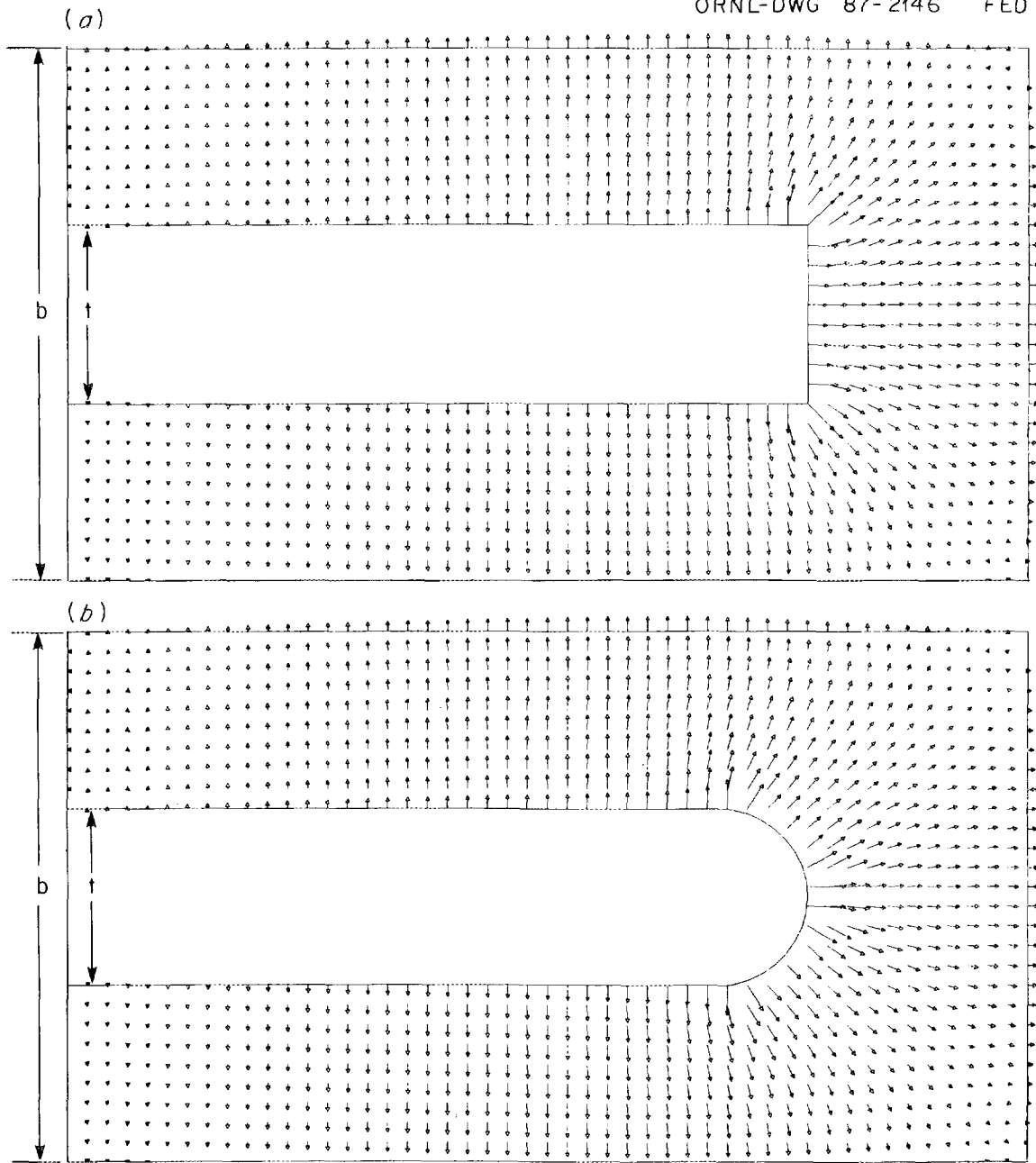


Fig. 9. The transverse electric field (\vec{E}_\perp) in a folded waveguide that has (a) vanes with rectangular tips and (b) vanes with semispherical tips.

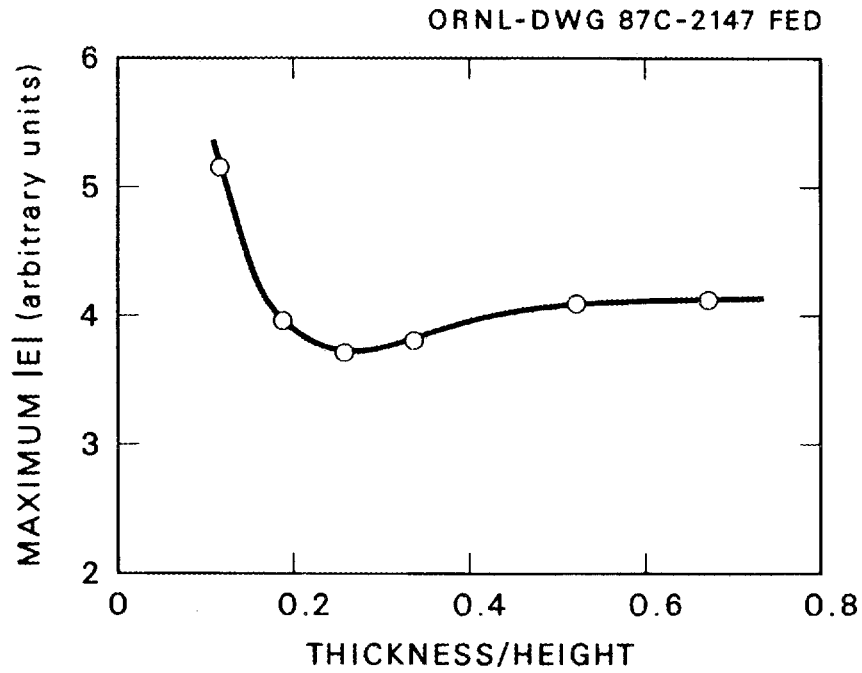


Fig. 10. Maximum $|E_{\perp}|$ of single-vane folded waveguide vs vane thickness. The gap between vane tip and wall is kept constant for this plot.

IV. CONCLUSIONS

We have investigated the character of the magnetic fields for the lowest frequency mode of the folded waveguide. The calculations are verified by experimental measurements. An approximate formula for the resonant frequency for the folded waveguide is given. The effects of the vane's geometrical shape on the field structure are discussed. This analysis can be used to design a high-power folded waveguide for ICRF plasma heating and to reduce the probability of voltage breakdown in the structure.

REFERENCES

- ¹T. L. Owens, IEEE Trans. Plasma Sci. **PS-14**, 934 (1986).
- ² W. L. Barrow and H. Schaevitz, AIEE Trans. **60**, 119 (1941).
- ³J. H. Whealton, G. L. Chen, R. J. Raridon, R. W. McGaffey, E. F. Jaeger, M. A. Bell, and D. J. Hoffman, "A 3-D analysis of Maxwell's equations for cavities of arbitrary shape," J. Comput. Phys., accepted for publication.
- ⁴W. J. R. Hofer, IEEE Trans. Microwave Theory Tech. **MT-33** (10), 882-893 (1985), and references therein.
- ⁵T. L. Owens and G. L. Chen, Fusion Technol. **10** (3), Part 2A, 1024 (1986).
- ⁶For example, W. K. H. Panofsky and M. Phillips, *Classical Electricity and Magnetism*, 2nd Ed. (Addison-Wesley, Reading, Mass., 1962), p. 225.

INTERNAL DISTRIBUTION

- | | | | |
|------|-----------------|--------|---|
| 1. | F. W. Baity | 22. | D. W. Swain |
| 2. | R. D. Burris | 23. | C. C. Tsai |
| 3. | B. A. Carreras | 24. | J. H. Whealton |
| 4-11 | G. L. Chen | 25. | T. L. White |
| 12. | R. A. Dory | 26. | J. Sheffield |
| 13. | H. H. Haselton | 27-28. | Laboratory Records Department |
| 14. | J. A. Holmes | 29. | Laboratory Records, ORNL-RC |
| 15. | E. F. Jaeger | 30. | Central Research Library |
| 16. | J. F. Lyon | 31. | Document Reference Section |
| 17. | R. C. Mann | 32. | Fusion Energy Division Library |
| 18. | J. K. Munro | 33-34. | Fusion Energy Division
Publications Office |
| 19. | L. W. Owen | 35. | ORNL Patent Office |
| 20. | T. L. Owens | | |
| 21. | D. J. Strickler | | |

EXTERNAL DISTRIBUTION

36. Office of the Assistant Manager for Energy Research and Development, U.S. Department of Energy, Oak Ridge Operations Office, P. O. Box E, Oak Ridge, TN 37831
37. J. D. Callen, Department of Nuclear Engineering, University of Wisconsin, Madison, WI 53706-1687
38. J. F. Clarke, Director, Office of Fusion Energy, Office of Energy Research, ER-50 Germantown, U.S. Department of Energy, Washington, DC 20545
39. R. W. Conn, Department of Chemical, Nuclear, and Thermal Engineering, University of California, Los Angeles, CA 90024
40. S. O. Dean, Fusion Power Associates, Inc., 2 Professional Drive, Suite 248, Gaithersburg, MD 20879
41. H. K. Forsen, Bechtel Group, Inc., Research Engineering, P. O. Box 3965, San Francisco, CA 94105
42. J. R. Gilleland, L-644, Lawrence Livermore National Laboratory, P.O. Box 5511, Livermore, CA 94550
43. R. W. Gould, Department of Applied Physics, California Institute of Technology, Pasadena, CA 91125

44. R. A. Gross, Plasma Research Laboratory, Columbia University, New York, NY 10027
45. D. M. Meade, Princeton Plasma Physics Laboratory, P.O. Box 451, Princeton, NJ 08544
46. M. Roberts, International Programs, Office of Fusion Energy, Office of Energy Research, ER-52 Germantown, U.S. Department of Energy, Washington, DC 20545
47. W. M. Stacey, School of Nuclear Engineering and Health Physics, Georgia Institute of Technology, Atlanta, GA 30332
48. D. Steiner, Nuclear Engineering Department, NES Building, Tibbetts Avenue, Rensselaer Polytechnic Institute, Troy, NY 12181
49. R. Varma, Physical Research Laboratory, Navrangpura, Ahmedabad 380009, India
50. Bibliothek, Max-Planck Institut für Plasmaphysik, Boltzmannstrasse 2, D-8046 Garching, Federal Republic of Germany
51. Bibliothek, Institut für Plasmaphysik, KFA Jülich GmbH, Postfach 1913, D-5170 Jülich, Federal Republic of Germany
52. Bibliothek, KfK Karlsruhe GmbH, Postfach 3640, D-7500 Karlsruhe 1, Federal Republic of Germany
53. Bibliotheque, Centre de Recherches en Physique des Plasmas, Ecole Polytechnique Federale de Lausanne, 21 Avenue des Bains, CH-1007 Lausanne, Switzerland
54. F. Prévot, CEN/Cadarache, Departement de Recherches sur la Fusion Contrôlée, F-13108 Saint-Paul-lez-Durance Cedex, France
55. Bibliothèque, CEN/Cadarache, F-13108 Saint-Paul-lez-Durance Cedex, France
56. Documentation S.I.G.N., Departement de la Physique du Plasma et de la Fusion Contrôlée, Association EURATOM-CEA, Centre d'Etudes Nucléaires, B.P. 85, Centre du Tri, F-38041 Grenoble, France
57. Library, Culham Laboratory, UKAEA, Abingdon, Oxfordshire, OX14 3DB, England
58. Library, JET Joint Undertaking, Abingdon, Oxfordshire OX14 3EA, England
59. Library, FOM-Instituut voor Plasmafysica, Rijnhuizen, Edisonbaan 14, 3439 MN Nieuwegein, The Netherlands
60. Library, Institute of Plasma Physics, Nagoya University, Chikusa-ku, Nagoya 464, Japan
61. Library, International Centre for Theoretical Physics, P.O. Box 586, I-34100 Trieste, Italy
62. Library, Centro Recherche Energia Frascati, C.P. 65, I-00044 Frascati (Roma), Italy
63. Library, Plasma Physics Laboratory, Kyoto University, Gokasho, Uji, Kyoto, Japan

64. Plasma Research Laboratory, Australian National University, P.O. Box 4, Canberra, A.C.T. 2601, Australia
65. Library, Japan Atomic Energy Research Institute, Tokai Research Establishment, Tokai, Naka-gun, Ibaraki-ken 311-02, Japan
66. Library, Japan Atomic Energy Research Institute, Naka Research Establishment, Naka-machi, Naka-gun, Ibaraki-ken, Japan
67. T. V. George, Plasma Technologies Branch, Division of Development and Technology, Office of Fusion Energy, Office of Energy Research, ER-531 Germantown, U.S. Department of Energy, Washington, DC 20545
68. G. M. Haas, Fusion Technologies Branch, Division of Development and Technology, Office of Fusion Energy, Office of Energy Research, ER-533 Germantown, U.S. Department of Energy, Washington, DC 20545
69. E. Oktay, Division of Confinement Systems, Office of Fusion Energy, Office of Energy Research, ER-55 Germantown, U.S. Department of Energy, Washington, DC 20545
70. H. S. Staten, Plasma Technologies Branch, Division of Development and Technology, Office of Fusion Energy, Office of Energy Research, ER-531 Germantown, U.S. Department of Energy, Washington, DC 20545
71. S. Park, 1540 Boelter Hall, University of California at Los Angeles, Los Angeles, CA 90024
72. L. Murray, MZ 800-10, GD/P, P.O. Box 2507, Pomona, CA 91767
73. W. L. Sadowski, Fusion Theory and Computer Services Branch, Division of Applied Plasma Physics, Office of Fusion Energy, Office of Energy Research, ER-541, Germantown, U.S. Department of Energy, Washington, DC 20545
74. D. W. Ross, Fusion Research Center, University of Texas, Austin, TX 78712
75. G. J. Morales, Department of Physics, University of California at Los Angeles, Los Angeles, CA 90024
- 76-136. Given distribution as shown in TIC-4500, Magnetic Fusion Energy (Category Distribution UC-426: Experimental Plasma Physics, UC-427: Theoretical Plasma Physics)

